Optics Letters

Inverse design fiber-to-chip couplers for the O- and C-bands

JULIAN PITA,[1,*] PAULO DAINESE,[2] AND MICHAËL MÉNARD[1]

[1]Department of Electrical Engineering, École de Technologie Supérieure (ÉTS), Montreal, QC H3C 1K3, Canada
[2]Corning Research & Development Corporation, One Science Drive, Corning, New York 14830, USA
*julian-leonel.pita-ruiz@etsmtl.ca

Received 25 November 2024; revised 5 February 2025; accepted 11 February 2025; posted 11 February 2025; published 10 March 2025

High-efficiency fiber-to-chip couplers are essential for high-performance optical interconnects. In this Letter, we experimentally demonstrate two inverse-designed silicon-on-insulator (SOI) couplers tailored for single-mode fibers (SMFs) in the C and O telecommunication bands. The O-band coupler represents the first, to the best of our knowledge, experimental demonstration of a topology-optimized coupler for this band while maintaining a minimum feature size of 120 nm. Both couplers operate at an 8° angle and are optimized for TE polarization. The C-band coupler achieves a coupling efficiency of -3.3 dB with a 3-dB bandwidth of 64 nm, while the O-band coupler reaches -3.4-dB efficiency over a 3-dB bandwidth spanning from 1292 nm to 1355 nm. Measuring 12 μm by 12 μm, these devices are designed using a single optimized silicon layer, reducing fabrication complexity and achieving efficiencies comparable to those of much larger high-performance grating couplers. Their compact size can increase integration density and contribute to reducing fabrication costs. Additionally, these couplers could be suitable for spatial division multiplexing (SDM) interconnects using multicore fibers, where the mode field diameter is compatible with single-mode fibers. They could also be used with multimode fiber configurations, where multiple couplers could be combined to generate higher-order modes.

https://doi.org/10.1364/OL.550095

Photonic integrated fiber-to-chip couplers enable a wide range of applications, including high-performance interconnects [1–3], heterogeneous integration [4,5], and sensing [6,7]. Surface and edge coupling methods are prominent among various approaches [8,9], with surface coupling particularly notable for its compatibility with wafer-level testing and its suitability for spatial division multiplexing using multicore and multimode fibers [10–13]. Despite their robustness, conventional grating couplers designed for surface coupling often occupy a significant area and exhibit reduced performance when miniaturized [14–16]. Grating design has evolved from phase matching to include apodized, subwavelength, and advanced 2D optimization methods [17–20]. Typically, these approaches start with an initial 2D grating design, followed by a focused 3D design that generally results in gratings multiple times larger than the core size of a conventional SMF. Inverse design has played a crucial role in the miniaturization of various photonic devices over the past decade, including antennas [21], wavelength and mode multiplexers [22,23], power splitters [24], polarizers [25,26], reflectors [27,28], and switches [29], among others. Despite these advancements, miniaturizing fiber-to-chip couplers remains challenging due to the large optimization areas, leading to high computational costs and time-intensive processes. A significant advancement in miniaturization was presented in [30], where two couplers were designed for multicore fibers with an 8-μm mode field diameter. These designs employed a two-stage approach: first, a topology optimization for the taper section was performed, followed by a 2D optimization of the grating profile. The first coupler features a footprint of 15 μm × 10 μm and achieves an efficiency of -3.8 dB at perpendicular coupling. The second coupler operates at a 10° coupling angle, achieving an efficiency of -2.9 dB with a footprint of 20 μm × 10 μm. For standard SMF, several devices have been proposed using a high refractive index polysilicon overlay. Zhou and Tsang [31] presented a grating coupler measuring 42 μm by 24 μm, designed using genetic algorithms to optimize the grating structure in the silicon and polysilicon layers. It achieves a coupling efficiency of -1.45 dB at a 0° coupling angle. Tong *et al.* [32] demonstrated a slightly smaller coupler, measuring 32 μm by 24 μm, which is also optimized via genetic algorithms but focused on the polysilicon layer to maximize performance, achieving an efficiency of -2.7 dB with a 1-dB bandwidth of 33 nm. Despite their high efficiency, these couplers still have a significant footprint because light is focused by bending the grating. In [33], a compact free-form coupler measuring 10 μm by 10 μm is showcased and designed utilizing topology optimization on both the silicon and polysilicon layers. It achieves an efficiency of -4.7 dB with a 3-dB bandwidth of 75 nm at a 0° coupling angle. Notably, in [33], an optimization was conducted across the entire silicon layer, whereas in [32], the optimization was performed on a partially etched section of the silicon layer.

Although topology optimization was employed previously for designing fiber-to-chip couplers in the C-band, only one demonstration was reported for SMF [33], and experimental results have yet to reach the performance levels typically achieved with large grating couplers designed using traditional methods. In this Letter, we introduce two freeform couplers, each measuring 12 μm by 12 μm, designed to operate in the C-band and O-band

Corrected 18 March 2025

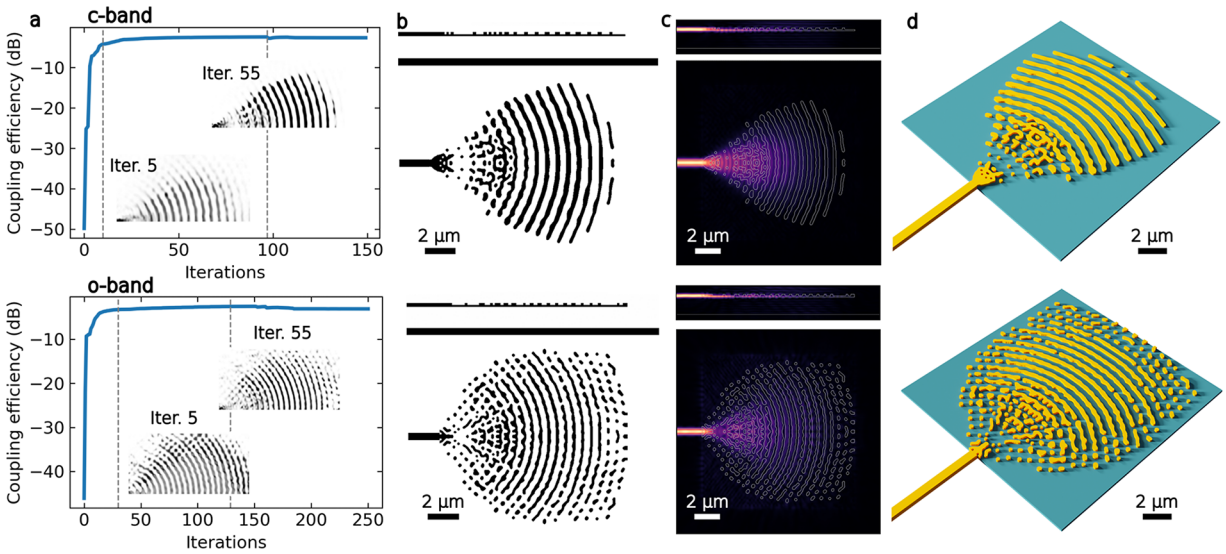

Fig. 1. Optimization process of both couplers, with the C-band coupler on top and the O-band coupler at the bottom. (a) Optimization trajectory showing the three stages of the optimization process and two insets displaying intermediate distributions of the refractive index. (b) Lateral and top views of the final geometry; the lateral view is a cross section through the middle of the coupler. (c) Electric field magnitude for the views shown in (b). (d) Schematic of the couplers illustrating the optimized layer and the bottom layer that remain as a silicon block.

with coupling angles of 8° and 10°, respectively, on a 250-nm thick SOI platform without a polysilicon overlay. The experimental results demonstrate a performance comparable to that of large grating couplers designed on similar platforms. However, it is important to note that a small radiated field profile of the couplers could reduce tolerance to alignment, increasing the complexity of packaging. These devices were designed using LumOpt with the L-BFGS optimizer in Ansys Lumerical, as it demonstrated strong robustness in the fabrication process, yielding high-performance and reproducible device structures. To control the size of the features, we set a minimum feature size of 120 nm. Additionally, the optimizer continuously smooths the geometry using a filter with a radius of 120 nm, which removes small features and rounds sharp corners. This approach ensures compatibility with commercial foundries. Simulation results show peak coupling efficiencies of -2.3 dB and -2.2 dB, with 3-dB bandwidths of 87 nm and 66 nm for the C-band and O-band couplers, respectively. Fabrication was carried out through a custom NanoSOI process using electron beam lithography. Experimental results reveal a peak efficiency of -3.3 dB with a 3-dB bandwidth spanning 64 nm for the C-band coupler, whereas the O-band coupler exhibited an efficiency of -3.4 dB over a 3-dB bandwidth of 63 nm. Both couplers could be used to couple high-order modes in few-mode fibers [34], and the O-band coupler could also be applied in multicore fibers, with 1×4 linear arrays of cores having a mode field diameter similar to that of SMF.

The couplers were designed for a platform consisting of a 250-nm-thick silicon layer, with a bottom cladding of 3 μm of silicon dioxide and a top cladding of 1 μm of silicon dioxide. The objective function aimed to maximize the coupling efficiency of the fundamental mode from a single-mode fiber to the fundamental TE mode of a waveguide with a width of 450 nm. The optimization spanned five wavelengths: 1540 nm, 1547.5 nm, 1550 nm, 1525 nm, and 1570 nm for the C-band and 1270 nm, 1285 nm, 1300 nm, 1315 nm, and 1330 nm for the O-band coupler. Throughout the optimization process, various optimization regions ranging from 9 μm × 9 μm to 12 μm × 12 μm were explored. It is important to note that larger optimization regions generally lead to improved device performance. Therefore, a 12 μm prototype was selected, exceeding the modal diameter of the SMF by at least one wavelength in both bands. To ensure reliable manufacturability, a minimum feature size of 120 nm was consistently maintained throughout t he optimization process, even though sizes as low as 100 nm are feasible. Additionally, several initial conditions were tested, including solid blocks of silicon, solid blocks of silicon dioxide, solid blocks with an average refractive index between silicon and silicon dioxide, and arbitrary refractive index distributions. Among these options, starting with a silicon dioxide block consistently demonstrated superior performance. This initial condition was therefore used to determine the size of the optimization region.

Figure 1 illustrates the results of the optimization process for both the C-band coupler (top) and the O-band coupler (bottom). The optimization was conducted on a 120-nm-thick silicon layer atop a 130-nm silicon layer, which remained intact. This thickness was chosen after evaluating various options ranging from 50 nm to 200 nm during 2D optimization processes. A 1-μm-thick silicon substrate layer was retained below the bottom cladding during the design process to account for its reflections. This approach significantly reduces the complexity of performing the optimization on two layers while still providing better performance. Symmetry in the problem was leveraged to reduce computational time. Figure 1(a) shows the optimization trajectory of both couplers, delineating the gray scale, binarization, and design-to-manufacturing (DFM) stages with dotted gray vertical lines. Both optimization paths progressed smoothly without the efficiency drop issues often encountered in topological optimization. The simulation time for the C-band coupler optimization was approximately 9 days on an Intel Core i7-9700 CPU with 64 GB of RAM, using 8 cores. On the other hand, the O-band coupler optimization took almost 10 days on the same system. The time per iteration varied from 40 min to nearly 3 h, with the final iterations during the design-to-manufacturing

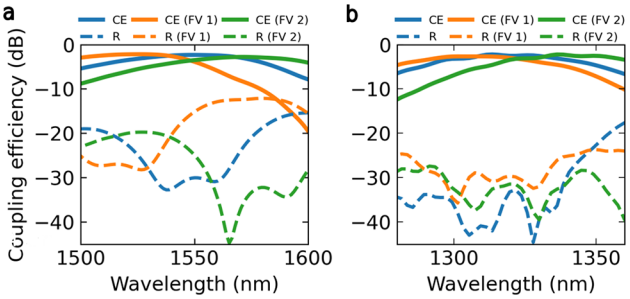

Fig. 2. Simulation results for the two couplers, including fabrication variations FV1 and FV2. (a) C-band coupler and (b) O-band coupler.

stage generally taking longer. The optimization process could be reduced to just a few days by using a cluster with a higher number of processors to speed up the FDTD simulations. The completed optimization yielded average coupling efficiencies of -2.6 dB for the C-band coupler and -3.1 dB for the O-band coupler. Notably, the optimization for the O-band coupler required 100 more iterations than for the C-band coupler. Insets in Fig. 1(a) depict the refractive index distributions at iterations 5 (gray scale) and 55 (binarization).

In Fig. 1(b), the geometries resulting from the optimization are presented in both profile and top views. These couplers exhibit significantly more complex shapes compared to traditional focused gratings, featuring subwavelength characteristics, especially near the waveguide. The middle sections show structures resembling rough grating teeth. Lateral views reveal that the coupler profiles in this section do not resemble apodized or regular gratings, making it challenging to derive a generic model. Interestingly, the O-band coupler, which resulted in an optimized structure larger in size than the C-band coupler, also exhibits more intricate characteristics toward the end of the coupler. This is unexpected given the larger modal field diameter of SMF in the C-band. Figure 1(c) depicts the electric field magnitude superimposed on the optimized device geometries in both profile and top views. It demonstrates effective confinement of the field within the waveguide, suggesting promising device performance. In Fig. 1(d), a scaled schematic of both couplers illustrates the two layers of the obtained devices: the 120-nm layer where topological optimization was conducted and the 130-nm layer that remained intact throughout the process.

Figure 2 presents simulation results for coupling efficiency and backreflections for the C-band and O-band couplers, with two fabrication variations (FVs) to assess the robustness of each coupler to fabrication deviations. FV1 corresponds to a lateral over-etching of approximately 8 nm of the optimized layer and of 10 nm in depth, whereas FV2 represents a lateral under-etching of about 8 nm and of 10 nm in depth. Additionally, both FVs include 10 nm of lateral misalignment between the optimized silicon layer and the input waveguide. These variations primarily affect the central wavelength rather than the peak coupling efficiency, shifting it toward shorter wavelengths for FV1 and toward longer wavelengths for FV2. Nevertheless, the 1-dB bandwidth of the devices remains greater than 41 nm for all FVs, mitigating the impact of the central wavelength shift. For instance, the C-band coupler is more sensitive to FV2. Under ideal conditions, it shows a coupling efficiency of -2.3 dB at 1548 nm, but under FV1, it shifts slightly to -2.2 dB at 1527 nm, whereas FV2 leads to a decrease to -2.7 dB at 1572 nm. In

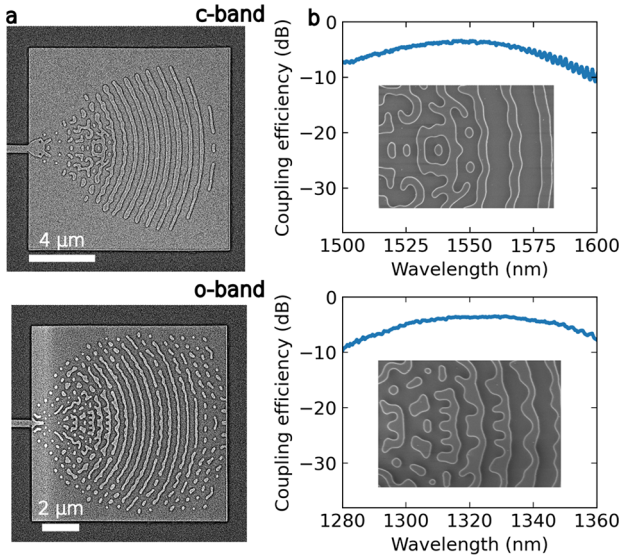

Fig. 3. Coupler results for the C-band (top) and O-band (bottom). (a) scanning electron microscopies (SEMs) images of the fabricated couplers. (b) Measured coupling efficiency, with an inset showing a zoomed-in portion of the SEM image.

contrast, the O-band coupler provides a coupling efficiency of -2.3 dB at 1313 nm under ideal conditions, but shifts to -2.6 dB at 1301 nm for FV1, and improves slightly to -2.2 dB at 1336 nm for FV2, suggesting a higher sensitivity to over-etching in FV1. The simulations further reveal that, under ideal conditions, reflections remain below -30 dB from 1532 nm to 1562 nm for the C-band coupler and from 1280 nm to 1339 nm for the O-band coupler. However, an increase in reflections is observed under both fabrication variations, particularly for the C-band coupler, which shows significantly higher reflections under the over-etching condition of FV1. It is worth noting that the effect of over- and under-etching depends on the feature size and feature density, resulting in fabrication variations that are more complex than uniform variations.

The couplers were fabricated using an electron beam lithography process at Applied Nanotools (ANT), as part of a custom silicon fabrication run. Partially etched devices were created through an anisotropic ICP-RIE process, followed by the deposition of a 1-μm silicon dioxide top cladding using a PECVD process. SEM images of the fabricated devices are shown in Fig. 3(a), demonstrating high fidelity to the designs depicted in Fig. 1(d). These images highlight the roughness of the grating teeth in the middle section, intricate details near the feed waveguide, and sub-wavelength features at the end of the O-band coupler. The couplers were characterized using an EXFO TC100S-HP tunable laser, a polarization controller to optimize TE mode coupling to the device under test (DUT), a 8° fiber array consisting of four SMFs, an EXFO CT440 tester, and a Thorlabs PM100 powermeter. Two identical couplers were connected in a loopback configuration, with each aligned to two fibers from the array. The output fiber was connected to either the tester or powermeter, depending on whether the O-band or C-band was being tested. The laser reference was obtained by accounting for losses through the polarization controller. The coupling efficiency was then determined by dividing the resulting measurement by two, assuming both couplers exhibited an identical performance.

Table 1. Comparison of Fiber-to-Chip Couplers for SMF Designed Using Topology Optimization Methods

Ref	Band	MFD (μm)	Coupling Angle (Meas)	Thickness (nm)	MFS (nm)	Footprint (μm^2)	CE (dB)		3-dB BW (nm)	
							Sim	Meas	Sim	Meas
[33]	C	10.4	0	-	-	100	−3.0	−4.7	73	75
This work	C	10.4	8	250	120	144	−2.3	−3.3	87	64
This work	O	9.2	8	250	120	144	−2.2	−3.4	66	63

Figure 3(b) presents the measured coupling efficiencies at 8° over a range of 1500 to 1600 nm for the C-band coupler and 1280 to 1380 nm for the O-band coupler.. As anticipated from the electric field distributions and simulations of fabrication robustness, both couplers achieve high efficiencies of -3.3 dB at 1547 nm for the C-band coupler and -3.4 dB at 1331 nm for the O-band coupler, with 3-dB bandwidths of 64 nm and 63 nm, respectively. The discrepancy between simulations and experimental results could be attributed to misalignment between the optimized layer and the bottom layer, as well as potential under-etching or over-etching during fabrication. Table 1 compares these compact couplers with others in the literature designed using a topology optimization method with SMF fibers. Compared to [33], our designs exhibit superior coupling efficiencies and lower simulated backreflections while utilizing only a 120-nm optimized silicon layer, which significantly reduces fabrication complexity, particularly with respect to the alignment between layers. Additionally, our C-band coupler demonstrates a smaller central wavelength shift of just 3 nm, achieving an efficiency of -3.5 dB at 1550 nm. This demonstrates that inverse design can produce compact and reproducible devices with performance comparable to those designed using traditional methods. Although the details of the silicon platform in [33] are not specified, it is important to note that they employ a polysilicon layer, which likely results in thicker couplers and a more complex fabrication process.

In summary, we investigated the topological optimization of silicon fiber-to-chip couplers for TE polarization. These couplers feature non-intuitive structures that are critical for achieving compactness and exceptional performance. With a compact footprint of 12 μm × 12 μm, the couplers achieve high efficiency, similar to that of typical large grating coupler devices, with -3.3 dB for the C-band coupler and -3.4 dB for the O-band coupler. Additionally, both couplers offer a 3-dB bandwidth exceeding 63 nm. These couplers could also be used for SDM interconnect applications, particularly in few-mode fibers, to couple high-order modes.

Funding. Natural Sciences and Engineering Research Council of Canada.

Acknowledgment. The authors thank Corning Inc. for their generous support, Applied Nanotools for fabrication assistance, and Aeponyx for providing access to the O-band tunable laser.

Disclosures. The authors have no conflicts of interest.

Data availability. Data underlying the results presented in this Letter are not publicly available at this time but may be obtained from the authors upon reasonable request.

REFERENCES

1. K. Y. Yang, C. Shirpurkar, A. D. White, *et al.*, Nat. Commun. **13**, 7862 (2022).
2. R. Zhang, X. Li, Y. He, *et al.*, Laser Photonics Rev. **17**, 2200750 (2023).
3. K. Lu, Z. Chen, H. Chen, *et al.*, Nat. Commun. **15**, 3515 (2024).
4. N. M. Jokerst, M. A. Brooke, S.-Y. Cho, *et al.*, IEEE J. Sel. Top. Quantum Electron. **9**, 350 (2003).
5. C. Xiang, W. Jin, D. Huang, *et al.*, IEEE J. Sel. Top. Quantum Electron. **28**, 8200515 (2022).
6. D. M. Kita, J. Michon, and J. Hu, Opt. Express **28**, 14963 (2020).
7. Y. Zhao, X.-g. Hu, S. Hu, *et al.*, Biosens. Bioelectron. **166**, 112447 (2020).
8. X. Mu, S. Wu, L. Cheng, *et al.*, Appl. Sci. **10**, 1538 (2020).
9. L. Cheng, S. Mao, Z. Li, *et al.*, Micromachines **11**, 666 (2020).
10. J. L. P. Ruiz, L. G. Rocha, J. Yang, *et al.*, Opt. Lett. **46**, 3649 (2021).
11. J. L. P. Ruiz, L. G. Rocha, J. Yang, *et al.*, Opt. Express **30**, 2539 (2022).
12. D. Yi, Y. Tong, and H. K. Tsang, J. Lightwave Technol. **42**, 287 (2024).
13. D. Yi, X. Zhou, and H. K. Tsang, IEEE Photonics J. **15**, 6602205 (2023).
14. D. S. Zemtsov, D. M. Zhigunov, S. S. Kosolobov, *et al.*, Opt. Lett. **47**, 3339 (2022).
15. F. Van Laere, T. Claes, J. Schrauwen, *et al.*, IEEE Photonics Technol. Lett. **19**, 1919 (2007).
16. R. Guo, S. Zhang, H. Gao, *et al.*, Photonics Res. **11**, 189 (2023).
17. Z. Zhao and S. Fan, J. Lightwave Technol. **38**, 4435 (2020).
18. M. K. Dezfouli, Y. Grinberg, D. Melati, *et al.*, Opt. Lett. **45**, 3701 (2020).
19. L. Su, R. Trivedi, N. V. Sapra, *et al.*, Opt. Express **26**, 4023 (2018).
20. A. Michaels and E. Yablonovitch, Opt. Express **26**, 4766 (2018).
21. J. L. Pita, I. Aldaya, P. Dainese, *et al.*, Opt. Express **26**, 2435 (2018).
22. A. Y. Piggott, J. Lu, K. G. Lagoudakis, *et al.*, Nat. Photonics **9**, 374 (2015).
23. W. Jiang, S. Mao, and J. Hu, Opt. Express **31**, 33253 (2023).
24. W. Chang, X. Ren, Y. Ao, *et al.*, Opt. Express **26**, 24135 (2018).
25. J. L. P. Ruiz, F. Nabki, and M. Ménard, Opt. Express **31**, 37892 (2023).
26. M. Perestjuk, H. Boerma, A. Schindler, *et al.*, IEEE Photonics Technol. Lett. **33**, 259 (2021).
27. Y. Kim and S.-H. Hong, Nanophotonics **13**, 2829 (2024).
28. J. Pita, F. Nabki, and M. Ménard, Opt. Lett. **49**, 786 (2024).
29. J. L. P. Ruiz, A. A. Rabih, S. Nabavi, *et al.*, in *2024 Optical Fiber Communications Conference and Exhibition (OFC)* (IEEE, 2024), pp. 1–3.
30. J. L. Pita Ruiz, L. G. Rocha, J. Yang, *et al.*, ACS Photonics **10**, 953 (2022).
31. X. Zhou and H. K. Tsang, Opt. Lett. **47**, 3968 (2022).
32. Y. Tong, W. Zhou, and H. K. Tsang, Opt. Lett. **43**, 5709 (2018).
33. A. M. Hammond, J. B. Slaby, M. J. Probst, *et al.*, Opt. Express **30**, 31058 (2022).
34. W. Zhang, M. Ye, Y. Li, *et al.*, IEEE Photonics J. **15**, 6600704 (2023).